Nitrogen-Oxyanion-Doped HfO_2 Resistive Random-Access Memory With Chemically Enhanced Forming

Ruofei Hu, Jianshi Tang, *Senior Member, IEEE*, Yue Xi, *Associate Member, IEEE*, Zhixing Jiang, Yuyao Lu, Bin Gao, *Senior Member, IEEE*, He Qian, and Huaqiang Wu, *Senior Member, IEEE*

***Abstract*— The high forming voltage of resistive random-access memory (RRAM) is one of the key bottlenecks for its integration in advanced silicon technology nodes. Here a nitrogen-oxyanion-doped (N-doped) hafnium oxide (HfO_2) RRAM with overall improvement on forming voltage, on/off ratio and endurance is demonstrated. The critical electric field of N-doped RRAM for forming is 40% less than that of undoped RRAM. Therefore, a thicker resistive switching layer (RSL) can be used to obtain the same forming voltage, which benefits the on/off ratio and endurance performance. The N-doped RRAM achieves 3× improvement in on/off ratio and 10× improvement in endurance at the forming voltage of 2 V, a value applicable for integration with advanced silicon technology node. We propose the hypothesis that the nitrites ($(NO_2)^-$) in the RSL of N-doped devices promote forming through introducing extra chemical process as well as additional conductive paths. Physical characterization and first-principles calculations are further carried out to validate our hypothesis.**

***Index Terms*— Resistive random-access memory (RRAM), nitrogen doping, chemically enhanced forming.**

I. Introduction

RESISTIVE random-access memory (RRAM) has been extensively studied due to its advantage in simple device structure, excellent compatibility with Si CMOS process for large-scale integration as well as high switching speed and low power [1], [2], [3]. The resistive switching characteristic of filamentary type RRAM attributes to the repeated growth and rupture of conductive filament (CF) inside the resistive switching layer (RSL). A large forming voltage, or critical electric field (∼5MV/cm for typical HfO_2 RRAM) is usually required to establish the CF at the beginning of operations [4], [5]. As CMOS keeps scaling, the required forming voltage also gradually increases due to narrow contact effect. Such a high forming voltage has become the bottleneck for integrating RRAM with advanced Si CMOS [6].

Various methods have been proposed to reduce the forming voltage of RRAM, including high temperature forming [7], energy band engineering [8], and material doping [9], [10], [11], [12], [13], [14], [15]. These methods, however, bring little change to the intrinsic electrochemical nature of forming. During forming, the oxygen atoms in the RSL get ionized, migrate under electric field and then combine with oxygen reservoir. This results in the formation of CF [16]. As a result, these methods often achieve optimization at the cost of increased process and operation complexity or degradation of other resistive switching characteristics such as on/off ratio and endurance.

In this work, we propose a novel nitrogen-oxyanion-doping (N-doping) method to improve the forming performance of HfO_2 RRAM. Different from previous doping methods, which use metallic element (Al [9], Mg [10], Ge [11], Ag [12]) dopants in the form of cations or non-metallic element (N [13], [14], F [15]) dopants in the form of anions, we use nitrogen oxyanions to dope HfO_2 RRAM. Magnetron sputtering is used to induce N-doping, where the high-energy plasma atmosphere promotes the chemical reactions between N, O and Hf. The N-dopants introduced extra chemical process as well as additional leakage paths to facilitate forming. The N-doped RRAM realizes a comprehensive improvement in forming voltage, on/off ratio and endurance. Physical experiments and first-principles calculations are performed to further investigate the mechanism of N-doping.

II. Experiments

In this work, a 1kb one-transistor-one-resistor (1T1R) array was fabricated to statistically study the characteristics of HfO_2 RRAM. Fig. 1(a) shows the schematic of the 1kb array, in which the transistors and peripheral circuits were fabricated using a standard 110 nm Si CMOS process. The size of RRAM is 700 × 700 nm^2. The length and width for the control transistor is 1 μm and 1.5 μm respectively. The RRAM stacks were deposited by magnetron sputtering (AJA ATC 2200-V). N-doping for HfO_2 was introduced by flowing N_2 together with O_2 to the chamber. The ratio of N_2 to O_2 is optimized as 9:1 to ensure a proper atomic concentration and chemical form of N-dopants. A capping layer of 0.7 mΩ·cm TaO_x was deposited on top of the RSL, serving as oxygen reservoir. The transmission electron microscope (TEM, Titan Themis G2) image of the RRAM is shown in Fig. 1(b). The chemical

Manuscript received 30 January 2023; revised 21 February 2023; accepted 25 February 2023. Date of publication 28 February 2023; date of current version 24 March 2023. This work was supported in part by the National Natural Science Foundation of China under Grant 92264201 and Grant 61974081; in part by the STI 2030-Major Projects under Grant 2022ZD0210200; and in part by the Center of Nanofabrication, Tsinghua University. The review of this letter was arranged by Editor S. Yu. *(Corresponding author: Jianshi Tang.)*

The authors are with the Beijing National Research Center for Information Science and Technology (BNRist), School of Integrated Circuits, Tsinghua University, Beijing 100084, China (e-mail: jtang@tsinghua.edu.cn).

Color versions of one or more figures in this letter are available at https://doi.org/10.1109/LED.2023.3250449.

Digital Object Identifier 10.1109/LED.2023.3250449

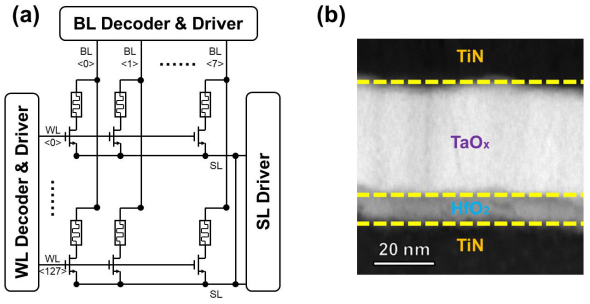

Fig. 1. (a) The schematic of the 1kb 1T1R RRAM array. (b) TEM image of TiN/TaO_x/HfO_2/TiN RRAM.

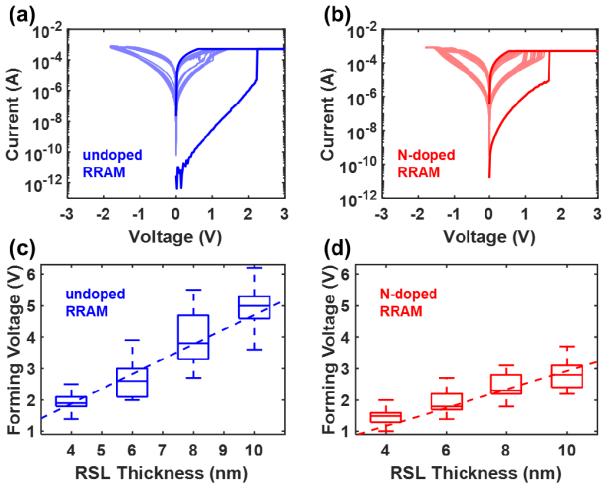

Fig. 2. The DC I-V curves of (a) undoped and (b) N-doped device with a RSL of 6 nm. The forming voltage obtained by pulse test of (c) undoped and (d) N-doped devices with different RSL thicknesses. 100 devices were tested in each batch.

composition of the HfO_2 layer was analyzed by X-ray photoelectron spectroscopy (XPS, AXIS Supra+). The electrical measurements were performed by Keysight B1500A for DC test and Speedcury ST2516 for pulse test. QuantumATK T-2022.03-SP1 [17] was used to perform molecular dynamics (MD) and density functional theory (DFT) calculations to further study the mechanism of N-doping.

III. Results and Discussion

Figs. 2(a) and (b) show the DC I-V curves of N-doped and undoped RRAM devices with a RSL of 6 nm, respectively. The N-doped device has a lower forming voltage (1.7 V) than the undoped device (2.3 V). Besides, both devices have similar operation voltages for set (1∼1.5 V) and reset (−1.4∼1.8 V). In practical applications, RRAM is operated by pulse rather than DC voltages. Therefore, we performed pulse test on the 1k RRAM array to obtain practical data of forming voltages. Here we utilized an incremental step pulse programming (ISPP) scheme [18] with a pulse width of 200 ns. The bit line (BL) voltage sweeps from 1 V to 6.4 V with a step of 0.1 V and the word line (WL) voltage sweeps from 0.7 V to 1.5 V with a step of 0.02 V. Since the thickness of RSL also affects the forming voltage [19], [20], RRAM devices with different RSL thicknesses were fabricated and tested for a comprehensive comparison. The results are shown in Fig. 2(c) for undoped devices and (d) for N-doped devices. The forming voltage is roughly in a linear relationship with the

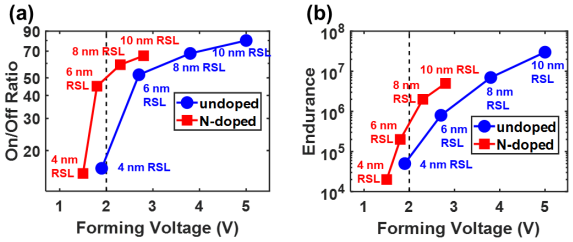

Fig. 3. Undoped devices and N-doped devices with different RSL thicknesses are tested to obtain (a) the forming voltage to on/off ratio tradeoff and (b) the forming voltage to endurance tradeoff. 100 and 50 devices in each batch were tested for on/off ratio and endurance respectively.

RSL thickness. From physics perspective, this is because the onset of forming process is determined by the electric field intensity in the RSL. The critical electric field of N-doped devices (2.9 MV/cm) is about 40% lower than that of undoped devices (4.7 MV/cm).

Although lower forming voltages can be easily obtained by decreasing the RSL thickness, it causes the degradation upon on/off ratio and endurance at the same time [7], [19], [20]. As the thickness of RSL decreases, fewer oxygen ions (O^{2-}) are driven by electric field and stored at the oxygen reservoir during forming. During the reset process, the devices with thin RSL would have fewer O^{2-} to be driven back to rupture CF, which results in a lower on/off ratio. Furthermore, electric field and heat generated in the reset process would also drive some of the stored O^{2-} to migrate to regions outside the CF, which results in the loss of stored O^{2-}. During the repeated set and reset processes, RRAM with thinner RSL would run out of stored O^{2-} more quickly, resulting in degraded endurance. [21] Therefore, N-doping allows RRAM to have a thicker RSL under the same forming voltage without sacrificing on/off ratio and endurance, achieving an overall enhanced performance.

Fig. 3 shows the comparison between undoped and N-doped devices on the tradeoff between forming voltage and on/off ratio (Fig. 3(a)) as well as endurance (Fig. 3(b)). The N-doped devices achieve comprehensive improvement on the trade-offs. At the forming voltage of 2 V, which is applicable for integration with 14 nm technology node according to [22], the N-dope devices achieve about 3× improvement on on/off ratio and 10× improvement on endurance. N-doped devices also show a relatively good retention. Fig. 4(a) compares the retention of N-doped and undoped devices. After being baked at 120°C for 1 hour, 95% of N-doped devices maintained an on/off ratio larger than 5× between the high- and low-resistance states (HRS/LRS). This percentage is close to that of undoped devices (96.5%).

To further investigate the role N-dopants played in forming, XPS was performed to identify the compound N formed. The XPS results for the RSL of N-doped devices are shown in Fig. 4(b). A peak at 403.9 eV is observed, indicating N-dopants are in the form of nitrites ($(NO_2)^-$) rather than nitrogen ion (N^{3-}). The atomic concentration of N is about 1.5%. It is speculated that $(NO_2)^-$ facilitate forming by absorbing oxygen and forming nitrates ($(NO_3)^-$) and oxygen vacancies (V_O) under electric field. The chemical equation is shown as follows:

$$0.5Hf^{4+} + (NO_2)^- + O^{2-} \xrightarrow{\vec{E}} 0.5Hf + (NO_3)^- + V_O^{2+} \quad (1)$$

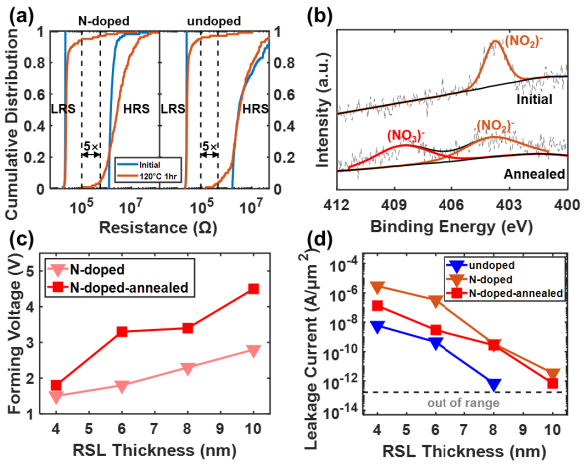

Fig. 4. (a) Retention of 100 N-doped and 100 undoped devices with 8 nm RSL. (b) XPS N1s spectra of N-doped devices. (c) Comparison of forming voltage after annealing for N-doped devices. (d) The pre-forming leakage current of undoped and doped devices, where the applied voltage is 0.5 V.

To verify this hypothesis, here we designed an annealing experiment, in which the RRAM devices were annealed at 300°C for 15 minutes. The annealing promoted $(NO_2)^-$ in N-doped devices to be oxidized into $(NO_3)^-$ (408.3 eV peak), as shown in Fig. 4(b). After annealing, the forming voltage of N-doped devices increased to a level similar to undoped devices (Fig. 4(c)). We can see the enhancement effect on forming by N-doping diminished as $(NO_2)^-$ turned into $(NO_3)^-$. These results prove that it is the $(NO_2)^-$ that played a vital role in forming. Although 300°C is much higher than the maximum local temperature of RRAM array during device operation [23], the thermal stability of $(NO_2)^-$ to some extent still limit the subsequent manufacturing process. This is not a serious problem because RRAM is integrated through low-temperature back-end-of-line (BEOL) process.

On the other hand, N-doping increases the pre-forming leakage current of RRAM (Fig. 4(d)), which also helps decrease the forming voltage. Larger leakage current indicates more leakage paths exist in the RSL of pre-forming N-doped devices. As a result, it is more likely to find a conductive path which is easier to form conductive filament during forming [25], [26]. The leakage current of N-doped devices decreased after annealing but was still higher than undoped devices (Fig. 4(d)), which in turn confirms that it is the combination of chemical process and leakage current that leads to the forming enhancement effect.

To further exploit the mechanism of N-doping, first-principles calculations were performed on a supercell of 146 atoms. The amorphous structure in Fig. 5(a) was generated by simulating melt-and-quench procedure in MD with a Morse potential set for HfO_2 [27]. The $(NO_2)^-$ dopant was established in accordance to the sp^2 hybridization of N. DFT simulation was carried out, with PseudoDojo pseudo-potentials [28] and generalized gradient approximation (GGA) based on Perdew–Burke–Ernzerhof (PBE) function [29], in order to extract the projected density of states (PDOS) for initial state (Fig. 5(b)) and final state (Fig. 5(c)) of chemical reaction (1). In the initial state, the $(NO_2)^-$ induced a deep impurity level in the energy bandgap. As the reaction generated a $(NO_3)^-$ and a V_O, the deep impurity level transformed into a shallow level in the final state, which was contributed by Hf atoms

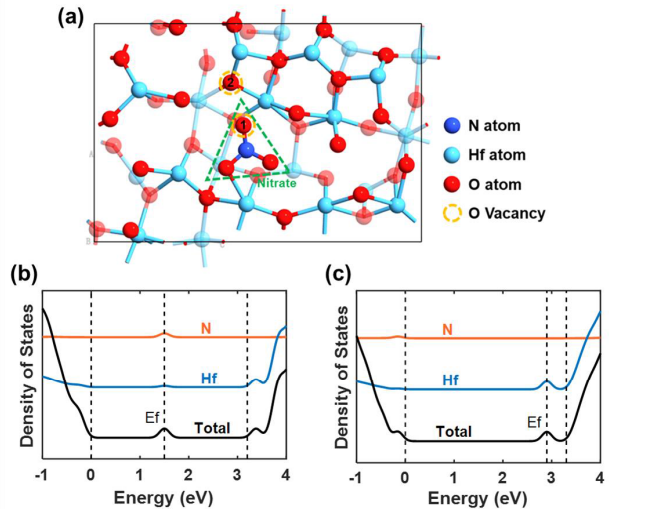

Fig. 5. (a) The atomic models of N-doped HfO_2 for DFT simulations. PDOS of (b) initial state and (c) final state of chemical reaction (1). The vacancy is placed at site 1 in the initial state, standing for a $(NO_2)^-$, and placed at site 2 in the final state, standing for a $(NO_3)^-$ together with a conductive V_O.

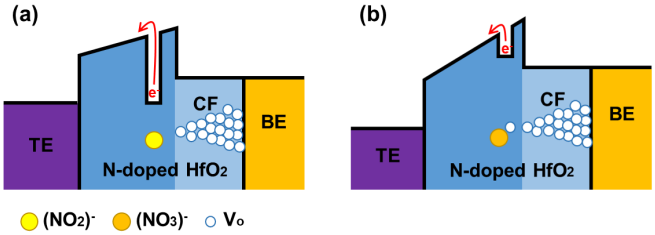

Fig. 6. The energy band diagram of N-doped devices in (a) the initial state and (b) the final state of reaction (1) during forming. The CF has a metallic conducting characteristic, of which the band structure is similar to the metal top electrode (TE) and bottom electrode (BE). [24].

near the V_O. The energy band diagram shown in Fig. 6 can be used to summarize the forming mechanism of N-doped devices. When the applied voltage is low, deep impurity level at the initial state induces multiple Poole-Frenkel emission and trap-assisted tunneling current paths, resulting in a large leakage current (Fig. 6(a)). When the applied voltage is large enough, reaction (1) is triggered and conductive V_O with a much lower barrier are formed, which then contribute to the growth of CF (Fig. 6(b)).

IV. Conclusion

In this work, we propose a novel N-doped HfO_2 RRAM with chemically enhanced forming. The N-doped RRAM has 40% lower critical forming electric field, which enables it to have a thicker RSL for the same forming voltage. It achieves 3× improvement of on/off ratio and 10× improvement of endurance at a forming voltage of 2 V that is applicable for integration with advanced nodes. The mechanism of N-doping is explained from both physical and chemical perspectives, which is validated by experiments and simulations. The N-doping method provides a new direction to improve the resistive switching characteristic of RRAM by inducing extra chemical process in forming.

References

[1] R. Waser and M. Aono, "Nanoionics-based resistive switching memories," *Nature Mater.*, vol. 6, no. 11, pp. 833–840, Nov. 2007, doi: 10.1038/nmat2023.

[2] M. Zangeneh and A. Joshi, "Design and optimization of nonvolatile multibit 1T1R resistive RAM," *IEEE Trans. Very Large Scale Integr. (VLSI) Syst.*, vol. 22, no. 8, pp. 1815–1828, Aug. 2014, doi: 10.1109/TVLSI.2013.2277715.

[3] B. Govoreanu, G. S. Kar, Y.-Y. Chen, V. Paraschiv, S. Kubicek, A. Fantini, I. P. Radu, L. Goux, S. Clima, R. Degraeve, N. Jossart, O. Richard, T. Vandeweyer, K. Seo, P. Hendrickx, G. H. P. Bender, L. Altimime, D. J. Wouters, J. A. Kittl, and M. Jurczak, "10×10 nm^2 Hf/HfO_x crossbar resistive RAM with excellent performance, reliability and low-energy operation," in *IEDM Tech. Dig.*, Dec. 2011, p. 31, doi: 10.1109/IEDM.2011.6131652.

[4] A. Beck, J. G. Bednorz, C. Gerber, C. Rossel, and D. Widmer, "Reproducible switching effect in thin oxide films for memory applications," *Appl. Phys. Lett.*, vol. 77, no. 1, pp. 139–141, 2000, doi: 10.1063/1.126902.

[5] X. Lian, X. Cartoixà, E. Miranda, L. Perniola, R. Rurali, S. Long, M. Liu, and J. Suñé, "Multi-scale quantum point contact model for filamentary conduction in resistive random access memories devices," *J. Appl. Phys.*, vol. 115, no. 24, Jun. 2014, Art. no. 244507, doi: 10.1063/1.4885419.

[6] H. Li, P. Huang, B. Gao, X. Liu, J. Kang, and H.-S. P. Wong, "Device and circuit interaction analysis of stochastic behaviors in cross-point RRAM arrays," *IEEE Trans. Electron Devices*, vol. 64, no. 12, pp. 4928–4936, Dec. 2017, doi: 10.1109/TED.2017.2766046.

[7] X. Xu, L. Tai, T. Gong, J. Yin, P. Huang, J. Yu, D. N. Dong, Q. Luo, J. Liu, Z. Yu, X. Zhu, X. L. Wu, Q. Liu, H. Lv, and M. Liu, "40× retention improvement by eliminating resistance relaxation with high temperature forming in 28 nm RRAM chip," in *IEDM Tech. Dig.*, Dec. 2018, p. 20, doi: 10.1109/IEDM.2018.8614593.

[8] A. Prakash, S. Maikap, H.-C. Chiu, T.-C. Tien, and C.-S. Lai, "Enhanced resistive switching memory characteristics and mechanism using a Ti nanolayer at the W/TaO_x interface," *Nanosc. Res. Lett.*, vol. 9, no. 1, p. 125, Dec. 2014, doi: 10.1186/1556-276X-9-152.

[9] M. Trapatseli, A. Khiat, S. Cortese, A. Serb, D. Carta, and T. Prodromakis, "Engineering the switching dynamics of TiO_x-based RRAM with Al doping," *J. Appl. Phys.*, vol. 120, no. 2, Jul. 2016, Art. no. 025108, doi: 10.1063/1.4958672.

[10] B. M. Long, S. Mandal, J. Livecchi, and R. Jha, "Effects of Mg-doping on HfO_2-based ReRAM device switching characteristics," *IEEE Electron Device Lett.*, vol. 34, no. 10, pp. 1247–1249, Oct. 2013, doi: 10.1109/LED.2013.2276482.

[11] Z. Wang, W. G. Zhu, A. Y. Du, L. Wu, Z. Fang, X. A. Tran, W. J. Liu, K. L. Zhang, and H.-Y. Yu, "Highly uniform, self-compliance, and forming-free ALD HfO_2-based RRAM with Ge doping," *IEEE Trans. Electron Devices*, vol. 59, no. 4, pp. 1203–1208, Apr. 2012, doi: 10.1109/TED.2012.2182770.

[12] C.-W. Wu, C.-C. Lin, P.-H. Chen, T.-C. Chang, K.-J. Zhou, W.-C. Chen, Y.-F. Tan, Y.-H. Yeh, S.-Y. Chou, H.-C. Huang, T.-M. Tsai, and S. M. Sze, "Realizing forming-free characteristic by doping Ag into HfO_2-based RRAM," *Appl. Phys. Exp.*, vol. 14, no. 4, Apr. 2021, Art. no. 041008, doi: 10.35848/1882-0786/abec58.

[13] E. R. Hsieh, K. T. Chen, P. Y. Chen, S. S. Wong, and S. S. Chung, "A FORMing-free HfO_2-/HfON-based resistive-gate metal–oxide–semiconductor field-effect-transistor (RG-MOSFET) nonvolatile memory with 3-bit-per-cell storage capability," *IEEE Trans. Electron Devices*, vol. 68, no. 6, pp. 2699–2704, Jun. 2021, doi: 10.1109/TED.2021.3074354.

[14] E. R. Hsieh, Y. X. Huang, Y. H. Ye, and Z. Y. Wang, "A three-bit-per-cell via-type resistive random access memory gated metal-oxide semiconductor field-effect transistor non-volatile memory with the FORMing-free characteristic," *Semicond. Sci. Technol.*, vol. 36, no. 12, Nov. 2021, Art. no. 124002, doi: 10.1088/1361-6641/ac33c3.

[15] M. Kim, Y. Wang, D.-E. Kim, Q. Shao, H.-S. Lee, and H.-H. Park, "Resistive switching properties for fluorine doped titania fabricated using atomic layer deposition," *APL Mater.*, vol. 10, no. 3, Mar. 2022, Art. no. 031105, doi: 10.1063/5.0076669.

[16] M. K. Yang, J.-W. Park, T. K. Ko, and J.-K. Lee, "Bipolar resistive switching behavior in $Ti/MnO_2/Pt$ structure for nonvolatile memory devices," *Appl. Phys. Lett.*, vol. 95, no. 4, Jul. 2009, Art. no. 042105, doi: 10.1063/1.3191674.

[17] S. Smidstrup, T. Markussen, P. Vancraeyveld, J. Wellendorff, J. Schneider, T. Gunst, B. Verstichel, D. Stradi, P. A. Khomyakov, U. G. Vej-Hansen, M.-E. Lee, S. T. Chill, F. Rasmussen, G. Penazzi, F. Corsetti, A. Ojanperä, K. Jensen, M. L. N. Palsgaard, U. Martinez, A. Blom, M. Brandbyge, and K. Stokbro, "QuantumATK: An integrated platform of electronic and atomic-scale modelling tools," *J. Phys., Condens. Matter*, vol. 32, no. 1, Jan. 2020, Art. no. 015901, doi: 10.1088/1361-648X/ab4007.

[18] K.-D. Suh, B.-H. Suh, Y.-H. Um, J.-K. Kim, Y.-J. Choi, Y.-N. Koh, S.-S. Lee, S.-C. Kwon, B.-S. Choi, J.-S. Yum, J.-H. Choi, J.-R. Kim, and H.-K. Lim, "A 3.3 V 32 Mb NAND flash memory with incremental step pulse programming scheme," in *IEEE Int. Solid-State Circuits Conf. (ISSCC) Dig. Tech. Papers*, Feb. 1995, pp. 128–129, doi: 10.1109/ISSCC.1995.535460.

[19] T. H. Park, S. J. Song, H. J. Kim, S. G. Kim, S. Chung, B. Y. Kim, K. J. Lee, K. M. Kim, B. J. Choi, and C. S. Hwang, "Thickness effect of ultra-thin Ta_2O_5 resistance switching layer in 28 nm-diameter memory cell," *Sci. Rep.*, vol. 5, no. 1, p. 15965, Nov. 2015, doi: 10.1038/srep15965.

[20] A. Bricalli, E. Ambrosi, M. Laudato, M. Maestro, R. Rodriguez, and D. Ielmini, "Resistive switching device technology based on silicon oxide for improved ON–OFF ratio—Part I: Memory devices," *IEEE Trans. Electron Devices*, vol. 65, no. 1, pp. 115–121, Jan. 2018, doi: 10.1109/ted.2017.2777986.

[21] B. Chen, Y. Lu, B. Gao, Y. H. Fu, F. F. Zhang, P. Huang, Y. S. Chen, L. F. Liu, X. Y. Liu, J. F. Kang, Y. Y. Wang, Z. Fang, H. Y. Yu, X. Li, X. P. Wang, N. Singh, G. Q. Lo, and D. L. Kwong, "Physical mechanisms of endurance degradation in TMO-RRAM," in *IEDM Tech. Dig.*, Dec. 2011, p. 12, doi: 10.1109/IEDM.2011.6131539.

[22] X. Xu, J. Yu, T. Gong, J. Yang, J. Yin, D. N. Dong, Q. Luo, J. Liu, Z. Yu, Q. Liu, H. Lv, and M. Liu, "First demonstration of OxRRAM integration on 14 nm FinFet platform and scaling potential analysis towards sub-10 nm node," in *IEDM Tech. Dig.*, Dec. 2020, doi: 10.1109/IEDM13553.2020.9371971.

[23] A. Ma, B. Gao, Y. Liu, P. Yao, Z. Liu, Y. Du, X. Li, F. Xu, Z. Hao, J. Tang, H. Qian, and H. Wu, "Multi-scale thermal modeling of RRAM-based 3D monolithic-integrated computing-in-memory chips," in *IEDM Tech. Dig.*, Dec. 2022, p. 15, doi: 10.1109/IEDM45625.2022.10019354.

[24] H.-S. P. Wong, H.-Y. Lee, S. Yu, Y.-S. Chen, Y. Wu, P.-S. Chen, B. Lee, F. T. Chen, and M.-J. Tsai, "Metal-oxide RRAM," *Proc. IEEE*, vol. 100, no. 6, pp. 1951–1970, Jun. 2012, doi: 10.1109/JPROC.2012.2190369.

[25] K. G. Young-Fisher, G. Bersuker, B. Butcher, A. Padovani, L. Larcher, D. Veksler, and D. C. Gilmer, "Leakage current-forming voltage relation and oxygen gettering in HfO_x RRAM devices," *IEEE Electron Device Lett.*, vol. 34, no. 6, pp. 750–752, Jun. 2013, doi: 10.1109/LED.2013.2256101.

[26] Z. Fang, X. P. Wang, J. Sohn, B. B. Weng, Z. P. Zhang, Z. X. Chen, Y. Z. Tang, G.-Q. Lo, J. Provine, S. S. Wong, H.-S. P. Wong, and D.-L. Kwong, "The role of Ti capping layer in HfO_x-based RRAM devices," *IEEE Electron Device Lett.*, vol. 35, no. 9, pp. 912–914, Sep. 2014, doi: 10.1109/LED.2014.2334311.

[27] G. Broglia, G. Ori, L. Larcher, and M. Montorsi, "Molecular dynamics simulation of amorphous HfO_2 for resistive RAM applications," *Model. Simul. Mater. Sci. Eng.*, vol. 22, no. 6, Sep. 2014, Art. no. 065006, doi: 10.1088/0965-0393/22/6/065006.

[28] M. J. van Setten, M. Giantomassi, E. Bousquet, M. J. Verstraete, D. R. Hamann, X. Gonze, and G.-M. Rignanese, "The PseudoDojo: Training and grading a 85 element optimized norm-conserving pseudopotential table," *Comput. Phys. Commun.*, vol. 226, pp. 39–54, May 2018, doi: 10.1016/j.cpc.2018.01.012.

[29] J. P. Perdew, K. Burke, and M. Ernzerhof, "Generalized gradient approximation made simple," *Phys. Rev. Lett.*, vol. 78, no. 7, p. 1396, Feb. 1997, doi: 10.1103/PhysRevLett.78.1396.